# Lattice dynamics and inelastic neutron scattering from sillimanite and kyanite $Al_2SiO_5$

Mala N. Rao,* S. L. Chaplot, Narayani Choudhury, and K. R. Rao
*Condensed Matter Physics Division, Bhabha Atomic Research Centre, Trombay, Mumbai-400085, India*

R. T. Azuah, W. T. Montfrooij, and S. M. Bennington
*ISIS Facility, Rutherford Appleton Laboratory, Chilton, Didcot, OXON OX11 0QX, United Kingdom*
(Received 25 February 1999; revised manuscript received 29 July 1999)

Sillimanite and kyanite are two of the polymorphs of aluminum silicate $Al_2SiO_5$, a geophysically important mineral system. Their crystal structures are characterized by chains of aluminum octahedra linked through aluminum, silicon, and oxygen atoms. We report experimental studies of the phonon densities of states of sillimanite and kyanite, and their interpretations based on shell model calculations. The inelastic neutron-scattering experiments were carried out both on a triple-axis spectrometer at the steady state reactor Dhruva (Trombay) as well as at a time-of-flight spectrometer at the ISIS spallation neutron source. The computed phonon densities of states are in good agreement with the experimental data and have been used to derive various macroscopic thermodynamic properties including the specific heat, equation of state, and atomic displacement parameters of sillimanite and kyanite. These studies have enabled an atomic level understanding of the phonon densities of states and resultant thermodynamic properties. [S0163-1829(99)02129-3]

## I. INTRODUCTION

One of the major goals of mineral physics is to develop the capability of predicting the physical and thermodynamic properties of minerals and their phase relations under various pressure-temperature conditions prevalent in the Earth. The key requirement for the prediction of the thermodynamic properties is the knowledge of the phonon density of states of these minerals. Earlier, by using a combination of inelastic neutron-scattering measurements and lattice dynamical calculations on forsterite $Mg_2SiO_4$, we could successfully predict the thermodynamical properties at high pressures and temperatures, such as the equation of state and the specific heat.[1,2]

The importance of the three $Al_2SiO_5$ aluminosilicates sillimanite, andalusite, and kyanite is well known in mineralogy.[3] The three polymorphs share a common feature in the crystal structure,[4] i.e., chains of $AlO_6$ edge-shared octahedra parallel to the crystallographic **b** axis. Sillimanite and andalusite have orthorhombic unit cells while kyanite has a triclinic unit cell. The transformations amongst the three $Al_2SiO_5$ polymorphs involve a change in primary coordination of one of the aluminum atoms, which is in tetrahedral coordination in sillimanite, five-coordinated in andalusite, and in octahedral coordination in kyanite. With the objective of studying the vibrational and thermodynamic properties of the $Al_2SiO_5$ polymorphs, we have undertaken detailed lattice dynamical studies of sillimanite and kyanite, involving extensive model calculations and experimental studies of the phonon density of states using the neutron inelastic scattering technique.

The crystal structures of sillimanite and kyanite have been studied using x-ray and neutron diffraction techniques, both at ambient as well as at high temperatures and pressures.[4–8] More recently, structure studies specific to the sites occupied by Al and Si have been carried out using electron energy loss spectroscopy,[9] x-ray photoelectron spectroscopy,[10] and x-ray absorption near-edge spectroscopy.[11] The elastic constants for sillimanite have been determined by ultrasonic techniques.[12] Infrared and Raman experimental data have been reported for sillimanite and kyanite, at room temperature, both at ambient pressure[13,14] and at high pressure.[15] Specific heat measurements up to 1000 K using calorimetry have been reported.[16–18]

Calculations of the equation of state and vibrational properties can be undertaken using quantum-mechanical and atomistic approaches. *Ab initio* density-functional studies of some silicate minerals including quartz $SiO_2$ and $MgSiO_3$ perovskite have been reported.[19–23] Similar studies have not been reported for the complex structures of the $Al_2SiO_5$ polymorphs sillimanite, andalusite, and kyanite. We have carried out detailed lattice dynamical calculations of sillimanite and kyanite using an atomistic approach involving interatomic potentials consisting of Coulomb and short-range terms. The calculations enabled microscopic interpretation of the experimental data and prediction of macroscopic properties such as specific heat and equation of state.

## II. CRYSTAL STRUCTURE AND LATTICE DYNAMICS

Sillimanite (space group *Pnma*) has an orthorhombic unit cell (Fig. 1) and four formula units per unit cell. It has seven atoms in the asymmetric unit with Al occupying two distinct crystallographic sites 4(a) and 4(c), which are in octahedral and tetrahedral coordinations, respectively. The other atoms are all located at 4(c), except for one oxygen atom, which is at the general position 8(d). Edge-shared $AlO_6$ octahedra run parallel to the **b** axis and a pair of such chains is linked to adjacent polyhedra through corner sharing. Kyanite (space group $P\bar{1}$; $Z=4$) has a triclinic unit cell (Fig. 1). The structure of kyanite is comprised of $AlO_6$ octahedra linked together by the remaining Al, Si, and O atoms. Also, kyanite has the smallest unit-cell volume of all the three polymorphs.

Models of the phonon density of states based on observed

 

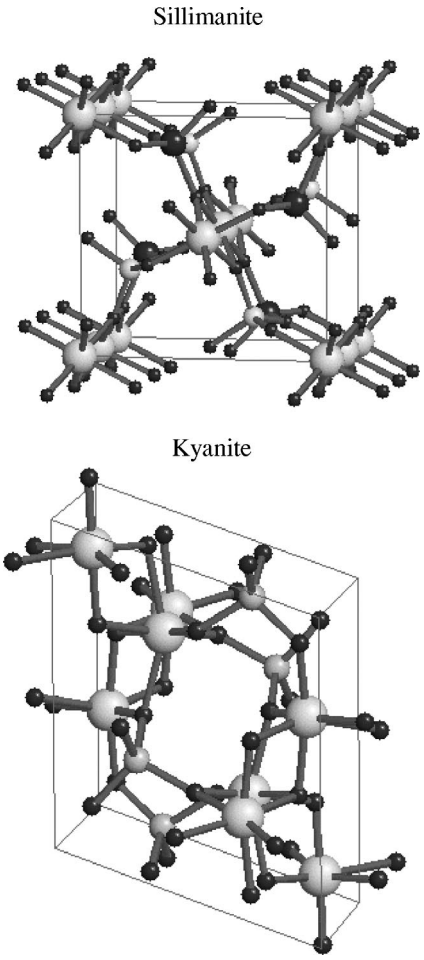


FIG. 1. Crystal structures of sillimanite and kyanite, $Al_2SiO_5$. The solid circles denote Al, Si, and O atoms in decreasing order of size. In sillimanite, Al1 is in octahedral coordination, while Al2 is in tetrahedral coordination.

Raman and infrared data have been employed to compute the thermodynamic properties of sillimanite and andalusite.[13] Lattice dynamical calculations of the high-symmetry phonons[24,25] and mean-square atomic displacements[25] of the three aluminosilicate minerals have also been reported. We have undertaken lattice dynamical calculations[26] using interatomic potentials consisting of Coulomb and short-range interactions and given by

$$V(r)=\left\{\frac{e^2}{4\pi\epsilon_o}\right\}\left\{\frac{Z(\kappa)Z(\kappa')}{r}\right\}+a\exp\left\{\frac{-br}{R(\kappa)+R(\kappa')}\right\}, \tag{1}$$

where $a=1822$ eV and $b=12.364$ (Refs. 1 and 27). $Z(\kappa)$ and $R(\kappa)$ are the effective charge and radius parameters associated with atom $\kappa$. The polarizability of the oxygen ions was modeled using the shell model, where a massless shell is linked to the core by harmonic interactions.

The covalent potential of the Si-O bond was simulated using the form

$$V(r)=-D\exp\left\{\frac{-n(r-r_0)^2}{2r}\right\}. \tag{2}$$

The calculations were undertaken using the computer program DISPR (Ref. 28) and the following optimized parameters: $Z(\mathrm{Al})=2.75$, $Z(\mathrm{Si})=3.00$, $Z(\mathrm{O})=-1.70$, $R(\mathrm{Al})=1.675$ Å, $R(\mathrm{Si})=1.40$ Å, $R(\mathrm{O})=1.70$ Å, oxygen shell charge$=-2.6e$, shell-core force constant$=110$ eV/Å$^2$, $D=1.2$ eV, $n=7.0$ Å$^{-1}$, and $r_0=1.627$ Å. These parameters give nearly vanishing forces on all the atoms as also positive eigenvalues of the dynamical matrix. At a given pressure and zero temperature, the free energy is minimized with respect to the structural variables, namely, the lattice parameters and the atomic positions. The equilibrium structure thus obtained is used in the lattice dynamics calculations.

We have carried out detailed group theoretical analysis of the phonon modes. For sillimanite, the phonon modes at the zone center $\Gamma$ point can be classified as

$$13A_g+8B_{1g}+13B_{2g}+8B_{3g}+11A_u$$
$$+16B_{1u}+11B_{2u}+16B_{3u}.$$

The $A_g$, $B_{1g}$, $B_{2g}$, and $B_{3g}$ modes are Raman active; the $B_{1u}$, $B_{2u}$, and $B_{3u}$ modes are infrared active and the $A_u$ modes are optically inactive. The group theoretical classification along the three high-symmetry directions is as follows:

$$\Sigma:\ 29\Sigma_1+19\Sigma_2+29\Sigma_3+19\Sigma_4,$$

$$\Delta:\ 24\Delta_1+24\Delta_2+24\Delta_3+24\Delta_4,$$

$$\Lambda:\ 29\Lambda_1+19\Lambda_2+19\Lambda_3+29\Lambda_4.$$

Using group theoretical information, the dynamical matrix was diagonalized along three high-symmetry directions and the normal modes were classified into different representations to give the phonon dispersion relation.

For kyanite, the phonon modes at the zone center $\Gamma$ point can be classified quite simply as

$$48A_g+48A_u.$$

The $A_g$ modes are Raman active while the $A_u$ modes are infrared active.

The phonon density of states is defined by the equation

$$g(\omega)=N\int_{\mathrm{BZ}}\sum_j\ \delta[\omega-\omega_j(\mathbf{q})]d\mathbf{q}, \tag{3}$$

where $N$ is a normalization constant such that $\int g(\omega)d\omega=1$; that is, $g(\omega)d\omega$ is the ratio of the number of eigenstates in the frequency interval $(\omega,\omega+d\omega)$ to the total number of eigenstates. $\omega_j(\mathbf{q})$ is the phonon frequency of the $j$th normal mode of phonon wave vector $\mathbf{q}$. The phonon density of states measured from inelastic neutron-scattering experiments is weighted with the neutron-scattering lengths of its constituent atoms. To compare with the experimental data, we have also computed the neutron weighted density of states given by

$$g^{(n)}(E)=\sum_k\ \left\{\frac{4\pi b_k^2}{m_k}\right\}g_k(E), \tag{4}$$

where $b_k$, $m_k$, and $g_k(E)$ are, respectively, the neutron-scattering length, mass, and partial density of states of the

TABLE I. Lattice constants (in Å), atomic fractional coordinates, and isotropic displacement parameters (in $Å^2$) of sillimanite. Experimentally determined values (at 298 K) are from Ref. 7.

| | | | | *a* | *b* | *c* | | |
|---|---|---|---|---|---|---|---|---|
| | | | Experimental | 7.6750 | 5.7751 | 7.4857 | | |
| | | | Calculated | 7.5828 | 5.9481 | 7.3498 | | |
| | Experimental | | | | Calculated | | | |
| | *x* | *y* | *z* | $B_{iso}$ | *x* | *y* | *z* | $B_{iso}$ |
| Al1 | 0.0 | 0.0 | 0.0 | 0.37 | 0.0 | 0.0 | 0.0 | 0.26 |
| Al2 | 0.3452 | 0.25 | 0.1417 | 0.44 | 0.3429 | 0.25 | 0.1278 | 0.30 |
| Si | 0.3404 | 0.75 | 0.1532 | 0.42 | 0.3317 | 0.75 | 0.1549 | 0.26 |
| O1 | 0.4089 | 0.75 | 0.3602 | 0.52 | 0.4010 | 0.75 | 0.3581 | 0.41 |
| O2 | 0.4339 | 0.25 | 0.3566 | 0.55 | 0.4367 | 0.25 | 0.3513 | 0.39 |
| O3 | 0.0009 | 0.75 | 0.4767 | 0.91 | 0.0089 | 0.75 | 0.4705 | 0.71 |
| O4 | 0.2232 | 0.5145 | 0.1255 | 0.63 | 0.2285 | 0.5225 | 0.1202 | 0.37 |

atomic species $k$ and $E=\hbar\omega$. The factor $(4\pi b_k^2/m_k)$ for the atoms Al, Si, and O is 0.0554, 0.0773, and 0.2645 barn/amu, respectively.

The calculated density of states was used to evaluate the specific heat at constant volume $C_v(T)$. The experimentally determined quantity is the specific heat at constant pressure $C_p(T)$. To compare with the experimental data, we have calculated the anharmonic corrections to the specific heat involving the difference $C_p(T)-C_v(T)$, which essentially depends on the bulk modulus and thermal expansion. The procedures adopted for the computation of these thermodynamic properties have been discussed earlier.[1,2]

## III. INELASTIC NEUTRON-SCATTTERING EXPERIMENTS

The natural samples of polycrystalline sillimanite and kyanite (weighing around 40 g each) used in our experiments were purified using chemical and magnetic separation methods at the Ore Dressing Section of the Bhabha Atomic Research Centre. Neutron diffraction was then used to ascertain the purity of this powder to be around 98%.

The neutron-scattering experiments were carried out first on a triple-axis spectrometer (TAS) on the steady-state reactor Dhruva (Trombay). At Trombay, the neutron inelastic scattering measurements were carried out at 300 K on a TAS with an overall energy resolution of 15%. Useful data were obtained for phonon energies below 45 meV. Above 45 meV the spectrum had significant contribution from second-order neutron energy gain processes at the crystal analyzer.

Inelastic neutron-scattering measurements were subsequently carried out on the multiangle rotor instrument (MARI) by the time-of-flight method. MARI is a direct geometry spectrometer for inelastic neutron scattering located at beam S6 on ISIS. It has a background suppression chopper and a Fermi chopper, which monochromatizes the beam. The detectors cover the angles from 3° to 135° and thus large regions of $(Q,\omega)$ space are covered concurrently in one measurement. Also, this instrument has an energy resolution of 1–2 % of the incident neutron energy at high energy transfers.

The measurements at ISIS were carried out with the sample at a temperature of 15 K. The sample was in the form of an annulus formed by aluminum foil; the thickness of the sample in the path of the beam was 5 mm, giving a sample transmission of approximately 90%. The energy of the incident neutrons was chosen to be around 180 meV. This enabled the measurement to cover a momentum-transfer range of 2–17 $Å^{-1}$.

Data analysis was done using standard programs available at ISIS. This analysis consisted of converting the as-measured data to $S(\phi,E)$ after corrections for background and sample container. It was converted to absolute scale by comparison with vanadium data taking into account the efficiency function of detectors. The neutron weighted phonon densities of states were obtained by suitably averaging the data over the scattering angles $\phi$.

## IV. RESULTS AND DISCUSSION

### A. Structure and elastic constants

The calculated structure parameters (Tables I and II) are quite close to those determined by diffraction experiments.[7] The calculated lattice parameters differ by less than 2% on average from the experimentally determined data at ambient temperature and pressure; also, for kyanite, the cell angles are calculated to within 0.4°. The computed elastic constants for sillimanite (Table III) also do not differ greatly from the experimentally observed values; on average, they deviate by about 10%.

### B. Phonon density of states

The experimental neutron weighted phonon densities of states of sillimanite and kyanite are shown in Fig. 2. The data are in good agreement with the TAS data (10–45 meV) obtained at the Dhruva reactor by Rao *et al.*[29] In order to extract the one-phonon density of states from the experimental data, the multiphonon contribution needs to be estimated. A monatomic approximation is often employed for this purpose. However, since the contributions arising from the different species of atoms are expected to be very different, the lattice dynamical model was used to compute the multiphonon contribution in the incoherent approximation using Sjolander's formalism.[1,30] Taking into account the calculated multiphonon contribution to the density of states at 15 K, the

TABLE II. Lattice constants (in Å), atomic fractional coordinates, and isotropic displacement parameters (in Å$^2$) of kyanite. Experimentally determined values (at 298 K) are from Ref. 7.

| | | *a* | *b* | *c* | $\alpha$ | $\beta$ | $\gamma$ | |
|---|---|---|---|---|---|---|---|---|
| | Experimental | 7.1200 | 7.8479 | 5.5738 | 89.974 | 101.117 | 106.00 | |
| | Calculated | 7.0967 | 7.9654 | 5.7359 | 90.60 | 101.63 | 106.06 | |
| | | Experimental | | | | Calculated | | |
| | *x* | *y* | *z* | $B_{iso}$ | *x* | *y* | *z* | $B_{iso}$ |
| Al1 | 0.3253 | 0.7041 | 0.4581 | 0.267 | 0.3472 | 0.7055 | 0.4613 | 0.353 |
| Al2 | 0.2974 | 0.6988 | 0.9504 | 0.258 | 0.2988 | 0.6988 | 0.9488 | 0.266 |
| Al3 | 0.0998 | 0.3862 | 0.6404 | 0.259 | 0.1039 | 0.3772 | 0.6302 | 0.289 |
| Al4 | 0.1121 | 0.9175 | 0.1647 | 0.273 | 0.1224 | 0.9291 | 0.1755 | 0.274 |
| Si1 | 0.2963 | 0.0649 | 0.7066 | 0.215 | 0.2925 | 0.0589 | 0.7158 | 0.213 |
| Si2 | 0.2910 | 0.3317 | 0.1894 | 0.216 | 0.2840 | 0.3351 | 0.1745 | 0.213 |
| O1 | 0.1093 | 0.1469 | 0.1287 | 0.384 | 0.1241 | 0.1506 | 0.1182 | 0.361 |
| O2 | 0.1229 | 0.6854 | 0.1811 | 0.302 | 0.1392 | 0.7019 | 0.1962 | 0.313 |
| O3 | 0.2751 | 0.4544 | 0.9547 | 0.349 | 0.2628 | 0.4549 | 0.9616 | 0.342 |
| O4 | 0.2835 | 0.9357 | 0.9357 | 0.334 | 0.2733 | 0.9297 | 0.9199 | 0.337 |
| O5 | 0.1084 | 0.1521 | 0.6667 | 0.342 | 0.1194 | 0.1521 | 0.6821 | 0.342 |
| O6 | 0.1219 | 0.6307 | 0.6394 | 0.297 | 0.1353 | 0.6242 | 0.6281 | 0.297 |
| O7 | 0.2823 | 0.4451 | 0.4287 | 0.346 | 0.2731 | 0.4368 | 0.4054 | 0.361 |
| O8 | 0.2916 | 0.9468 | 0.4657 | 0.346 | 0.2836 | 0.9515 | 0.4833 | 0.382 |
| O9 | 0.5007 | 0.2752 | 0.2441 | 0.364 | 0.4927 | 0.2893 | 0.2407 | 0.337 |
| O10 | 0.5015 | 0.2310 | 0.7560 | 0.350 | 0.4942 | 0.2152 | 0.7571 | 0.332 |

experimental neutron weighted one-phonon density of states $g^{(n)}_{exp}(E)$ was extracted (Fig. 2, dashed line). Using the ratio between the calculated density of states $g_{cal}(E)$ and the calculated neutron weighted density of states $g^{(n)}_{cal}(E)$ (Fig. 2) along with $g^{(n)}_{exp}(E)$, we determined the experimental one-phonon density of states $g_{exp}(E)$ (see Sec. IV E below).

The experimental densities of states have been interpreted on the basis of our lattice dynamical calculations. The calculated spectra have been broadened with a uniform instrumental resolution of 2 meV. The computed phonon densities of states are in good agreement with the experimental data. The partial density of states contains information concerning the vibrational behavior of each atom and involves phonons in the entire Brillouin zone. In sillimanite, the computed partial density of states (Fig. 3) reveals distinct contributions from the crystallographically inequivalent Al atoms with Al1 (in octahedral coordination) vibrations spanning 0–80 meV, while Al2 (in tetrahedral coordination) vibrations span 0–100 meV. The Si atoms in tetrahedral coordination contribute substantially in the spectral range above 100 meV.

TABLE III. Comparison of calculated and experimental (Ref. 12) elastic constants $C_{ij}$ (GPa) for sillimanite.

| | Experimental | Calculated | |
|---|---|---|---|
| | | Present work | Ref. 24 |
| $C_{11}$ | 232 | 284 | 277 |
| $C_{22}$ | 388 | 497 | 539 |
| $C_{33}$ | 287 | 275 | 285 |
| $C_{44}$ | 81 | 82 | 89 |
| $C_{55}$ | 89 | 73 | 85 |
| $C_{66}$ | 122 | 119 | 130 |

The O atom vibrations are significantly more anisotropic with large band gaps in their partial density of states. In kyanite, the computed partial density of states (Fig. 4) reveal contributions from Al (all of which are in octahedral coordination) in the range 0–100 meV, while the Si and O contribute in the entire spectral range from 0 to 140 meV. The partial density of states was used to compute the mean-square atomic displacements, which are in good qualitative agreement with available experimental data (Tables I and II).

### C. Thermodynamic properties

The computed specific heat is in excellent agreement with experimental values[16–18] (within 1%) over a wide range of temperature up to 1500 K (Fig. 5). The calculated anharmonic correction $(C_p - C_v)$ to the specific heat is less than 1% at 1500 K for sillimanite, whereas it is quite significant for kyanite (about 2% around 1000 K). The specific heat curves for the two minerals are very similar; the differences in low-temperature (below 300 K) specific heat will be discussed later in some detail. The calculated equations of state for sillimanite and kyanite are compared with the experimental data[7] in Figs. 6 and 7, respectively. All three unit-cell dimensions decrease with pressure. The compressibility is anisotropic; in sillimanite, the *b* axis is the least compressible, whereas *b* and *c* are nearly equally compressible in kyanite.

### D. Phonon dispersion relations

The theoretically calculated phonon dispersion curves for sillimanite along the three high-symmetry directions in the Brillouin zone $\Sigma$, $\Delta$, and $\Lambda$ are shown in Fig. 8. Since there are 32 atoms in the unit cell, there are 96 phonon branches

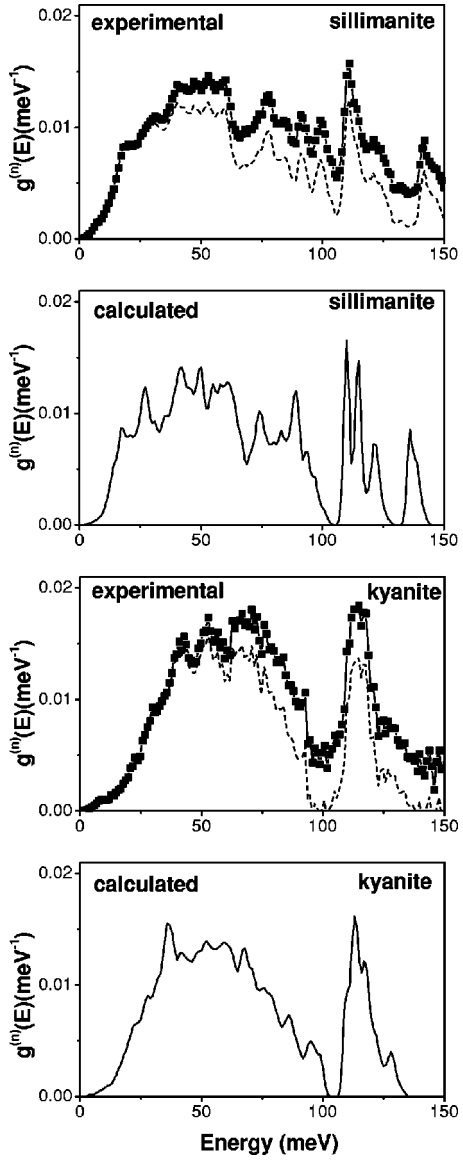


FIG. 2. Neutron weighted phonon density of states of sillimanite and kyanite. The experimental inelastic neutron-scattering data (squares) at $T=15$ K include one-phonon and multiphonon contributions; the errors in the data are less than the symbol size. The multiphonon contributions have been estimated and the experimental one-phonon neutron weighted density of states (dashed lines) so obtained can be directly compared with our calculations. The calculated spectra have been broadened with an instrumental resolution of 2 meV.

along each direction. The optic-phonon branches show moderate dispersion along the $\Sigma$ and $\Lambda$ directions and a larger dispersion along the $\Delta$ direction. In all the three directions, the branches are distributed almost uniformly up to 80 meV, but there is a distinct energy gap around 100 meV. This energy gap is more prominent in branches of the $\Sigma_2,\Sigma_4$ and $\Lambda_2,\Lambda_4$ representations. The phonon dispersion relation has been used to obtain one-phonon coherent neutron inelastic scattering cross sections for a single crystal. The calculated cross sections would greatly facilitate an experimental determination of the phonon dispersion relation using neutron inelastic scattering, subject to the availability of a good single crystal.

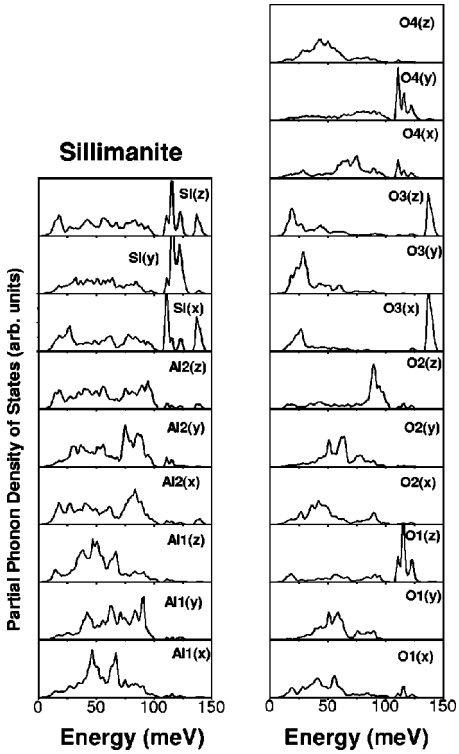


FIG. 3. Computed partial phonon density of states of the atoms Al1, Al2, Si, O1, O2, O3, and O4 along the three directions *x*, *y*, and *z* in sillimanite. The notation is consistent with Table I.

For kyanite, we have calculated the phonon dispersion curves along the three directions [100], [010], and [001]; they reveal that the branches have very small dispersion, except for the acoustic branches. Further, the optic branches are very close together almost forming a continuum in the region 20–100 meV but showing a distinct gap around 100 meV, as is evident also from the density of states.

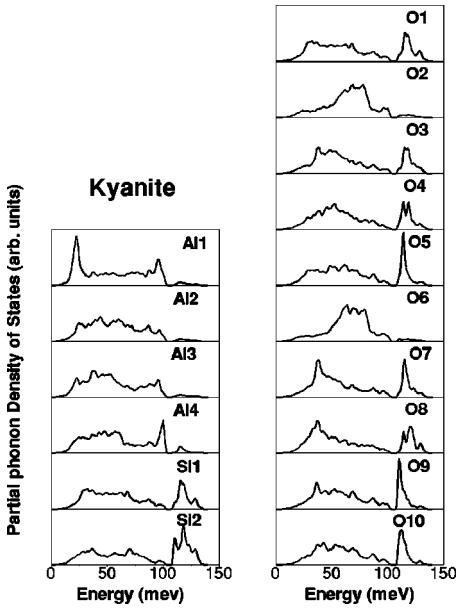


FIG. 4. Calculated partial phonon density of states of the various atoms in kyanite. The notations of atoms are consistent with Table II.

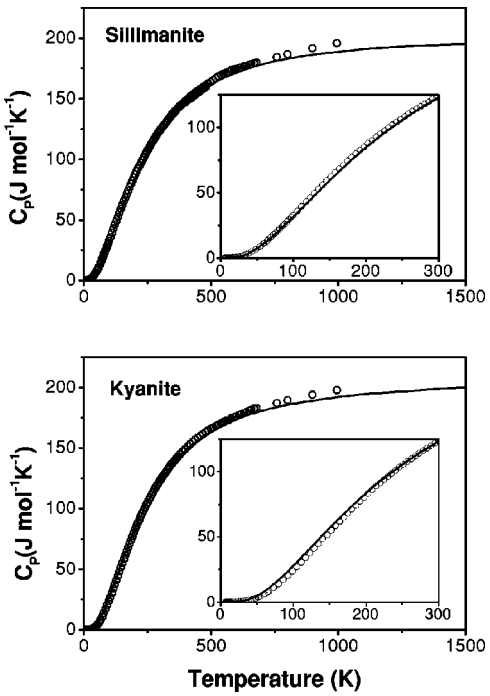


FIG. 5. Specific heat of sillimanite and kyanite, as a function of temperature. Symbols represent measured data from Refs. 17 and 18. The solid line is the model calculation. Insets show the low-temperature specific heat on an expanded scale.

### E. Comparisons of the vibrational and thermodynamic properties of sillimanite and kyanite

It is of interest to study how the structural differences between sillimanite and kyanite manifest in their vibrational properties. These two polymorphs of $Al_2SiO_5$ have different crystal structures: kyanite is triclinic, while sillimanite is orthorhombic. Our transferable shell-model potential has been able to reproduce the equilibrium structures (with minimum free energy) as well as the coordination of the Al atoms. The experimental one-phonon density of states for kyanite is compared with that of sillimanite in Fig. 9. In spite of the overall similarities, we can see that compared to sillimanite, the energy range of the phonon density of states in kyanite is reduced. Sillimanite has one extra peak at 145 meV. Further, in the region around 60 meV, sillimanite has lower density of states than kyanite. The contributions from low-frequency phonons (below 25 meV) significantly affect the low-temperature specific heat. In this region, the experimental density of states of kyanite is less than that of sillimanite. All these features are fairly reproduced in our calculations (Fig. 9). The differences in the phonon density of states of the two minerals manifest in their thermodynamic properties.

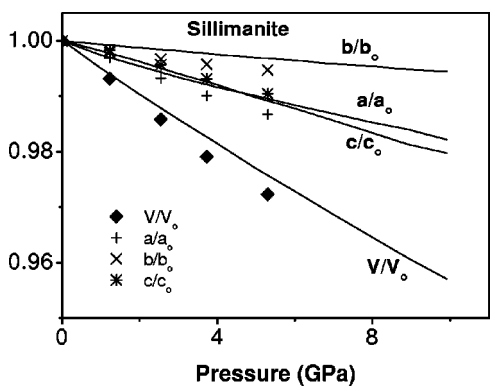


FIG. 6. Computed (solid line) fractional change in lattice parameters and volume with pressure, in sillimanite. Experimental values (symbols) are from Ref. 7.

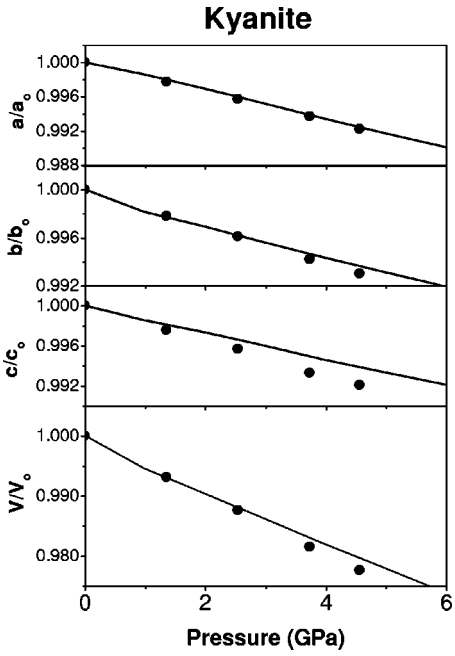


FIG. 7. Computed (solid line) fractional change in lattice parameters and volume with pressure, in kyanite. Experimental values (symbols) are from Ref. 7.

Figure 10 shows the difference in specific heats $C_p$(sillimanite)$-C_p$(kyanite) as a function of temperature. Kyanite has lower specific heat up to temperatures of about 300 K. This trend is reproduced in the estimates from the neutron data as well as the model calculations. However, the absolute values of the difference in the specific heat are very small (about 4 J mol$^{-1}$ K$^{-1}$; see Fig. 5) and perhaps cannot be accurately estimated using the present approach.

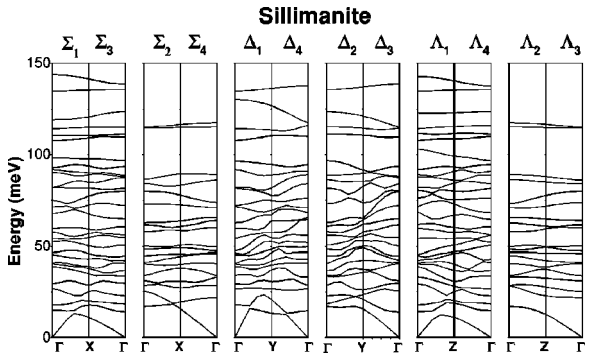


FIG. 8. Computed phonon dispersion curves for sillimanite along the three high-symmetry directions. Group theoretical representations are indicated on top of the figure. $\Gamma$ is the Brillouin zone center and $X$, $Y$, $Z$ are the zone boundary points along the $\Sigma$, $\Delta$, and $\Lambda$ directions, respectively.

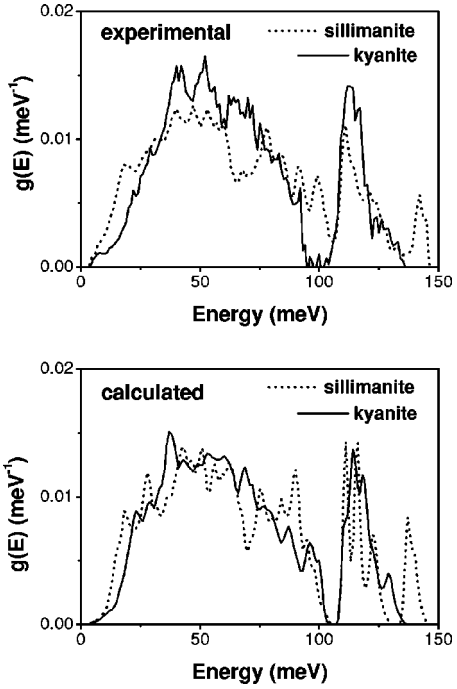


FIG. 9. Comparison of the one-phonon density of states of kyanite and sillimanite; experimental (upper) and calculated (lower).

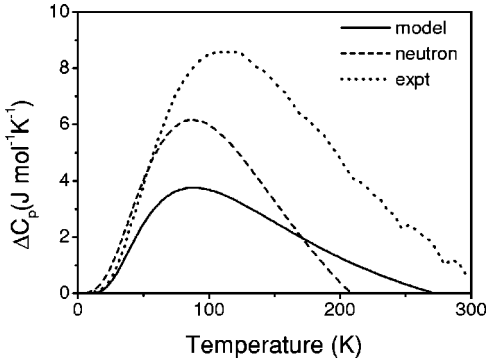


FIG. 10. The specific heat difference $\Delta C_p = C_p$(sillimanite) $- C_p$(kyanite) as a function of temperature. The full line shows the model calculation. The dashed line is an estimate using the phonon density of states $g_{exp}(E)$ derived from inelastic neutron-scattering measurements. The experimental curve (dotted line) has been obtained from specific heat data reported in Ref. 17.

## V. CONCLUSIONS

In this paper, we have reported inelastic neutron-scattering measurements of the phonon densities of states of polycrystalline samples of sillimanite and kyanite after having characterized them using optical microscope and neutron diffraction. The neutron measurements were carried out both on a triple-axis spectrometer at a steady-state reactor as well as on a time-of-flight spectrometer at a spallation neutron source. The measured neutron weighted phonon density of states agrees very well with that calculated through lattice dynamics using a shell model. The calculated phonon density of states has been interpreted microscopically on the basis of the partial density of states. The calculated crystal structure, the equation of state, elastic constants, and specific heat are in fair agreement with available experimental data. The model enabled predictions of the phonon dispersion relations and the equations of state of sillimanite and kyanite.

## ACKNOWLEDGMENTS

We are grateful to Dr. N. Krishna Rao and his colleagues at the Ore Dressing Section, BARC for making available pure samples. The natural sample of kyanite was obtained courtesy of Dr. R.S. Rawat, Wadia Institute of Himalayan Geology, Dehra Dun, India. We also thank Dr. S.K. Roy of the Metallurgy Division, BARC, for providing the initial sillimanite samples.

*FAX: 91 22 5505151. Electronic address: tassspd@apsara.barc.ernet.in

[1] K. R. Rao, S. L. Chaplot, Narayani Choudhury, Subrata Ghose, J. M. Hastings, L. M. Corliss, and D. L. Price, Phys. Chem. Miner. **16**, 83 (1988).
[2] N. Choudhury, S. L. Chaplot, and K. R. Rao, Phys. Chem. Miner. **16**, 599 (1989).
[3] D. M. Kerrick, *Reviews in Mineralogy* (Mineralogical Society of America, Washington, D.C., 1990), Vol. 22.
[4] J. K. Winter and S. Ghose, Am. Mineral. **64**, 573 (1979).
[5] C. W. Burnham, Z. Kristallogr. **118**, 127 (1963).
[6] L. W. Finger and E. Prince, Carnegie Inst. Wash. Publ. **71**, 496 (1972).
[7] Hexiong Yang, Robert T. Downs, Larry W. Finger, Robert M. Hazen, and Charles T. Prewitt, Am. Mineral. **82**, 467 (1997); H. Yang, R. M. Hazen, L. W. Finger, C. T. Prewitt, and R. T. Downs, Phys. Chem. Miner. **25**, 39 (1997).
[8] Paola Comodi, Pier Francesco Zanazzi, Stefano Poli, and Max W. Schmidt, Am. Mineral. **82**, 452 (1997).
[9] J. Tafto, Nucl. Instrum. Methods Phys. Res. B **2**, 733 (1984).
[10] K. B. Garg, P. Srivastava, N. L. Saini, S. Venkatesh, G. L. Dwivedi, S. Fernandes, G. S. Sekhawat, and R. P. Gupta, Indian J. Pure Appl. Phys. **33**, 530 (1995).
[11] M. Froba, Joe Wong, M. Rowen, G. E. Brown, Jr., T. Tanaka, and Z. Rek, Physica B **208&209**, 555 (1995).
[12] M. T. Vaughan and D. J. Weidner, Phys. Chem. Miner. **3**, 133 (1978).
[13] E. Salje and Chr. Werneke, Contrib. Mineral. Petrol. **79**, 56 (1982).
[14] Paul McMillan and Bernard Piriou, J. Non-Cryst. Solids **53**, 279 (1982).
[15] T. P. Mernagh and Lin-gun Liu, Phys. Chem. Miner. **18**, 126 (1991).
[16] E. Salje, Am. Mineral. **71**, 1366 (1986).
[17] Richard A. Robie and Bruce S. Hemingway, Am. Mineral. **69**, 298 (1984).
[18] B. S. Hemingway, R. A. Robie, H. T. Evans, Jr., and D. M. Kerrick, Am. Mineral. **76**, 1597 (1991).
[19] X. Gonze, D. C. Allan, and M. P. Teter, Phys. Rev. Lett. **68**, 3603 (1992).
[20] R. M. Wentzcovitch, J. L. Martins, and G. D. Price, Phys. Rev. Lett. **70**, 3947 (1993).
[21] R. M. Wentzcovitch, D. A. Hugh Jones, R. J. Angel, and G. D. Price, Phys. Chem. Miner. **22**, 453 (1995).
[22] L. Stixrude and R. E. Cohen, Nature (London) **364**, 613 (1993).
[23] B. B. Karki, L. Stixrude, S. J. Clark, M. C. Warren, G. J. Ack-

land, and J. Crain, Am. Mineral. **82**, 635 (1997).
[24] B. Winkler, M. T. Dove, and M. Leslie, Am. Mineral. **76**, 313 (1991).
[25] Tullio Pilati, Francesco Demartin, and C. M. Gramaccioli, Acta Crystallogr., Sect. B: Struct. Sci. **53**, 82 (1997).
[26] See P. Bruesch, in *Phonons: Theory and Experiments I*, Springer Series in Solid State Sciences Vol. 34 (Springer, Berlin, 1982); G. Venkataraman, L. A. Feldkamp, and V. C. Sahni, in *Dynamics of Perfect Crystals* (MIT Press, Cambridge, MA, 1975).
[27] S. L. Chaplot and K. R. Rao, J. Phys. C **16**, 3045 (1983).
[28] S. L. Chaplot (unpublished).
[29] Mala N. Rao, S. L. Chaplot, Narayani Choudhury, and K. R. Rao, Solid State Phys. (India) **37C**, 98 (1994).
[30] A. Sjolander, Ark. Fys. **14**, 315 (1958).